Hamadi, D., Ayoub, A. & Maalem, T. (2016). A new strain-based finite element for plane elasticity problems. Engineering Computations, 33(2), pp. 562-579. doi: 10.1108/EC-09-2014-0181

A New Strain-Based Finite Element for Plane Elasticity Problems

ABSTRACT

In this paper, a new quadrilateral strain-based element is developed. The element has five nodes, four at the corners as well as an internal node. Through the introduction of the internal node, the numerical performance of the element proved to be superior to existing elements, even though a static condensation is required. From several numerical examples, it is shown that convergence can be achieved with the use of only a small number of finite elements. The proposed element can be used to solve general plane elasticity problems resulting in excellent results. The results obtained are comparable with those given by the robust element Q8.

KEY WORDS: Strain-based, Quadrilateral element, Static condensation, Analytical integration.

1. Introduction

Since 1983, the strain-based finite element approach has been formulated by Sabir et al [1-3] to analyze general plane elasticity problems. Among these elements is the SBRIE (Strain-Based Rectangular In-plane Element) and SBRIE1 (Strain-Based Rectangular In-plane Element with An Internal Node) elements [4]. SBRIE assumes a linear variation of the direct strains and constant variation of the shear strain, while SBRIE1 assumes a linear variation of all three strain components. Unfortunately these elements can only be used for a regular form with appropriate coordinates, which tend to decrease the element's use for practical problems.

In this paper, a simple and efficient quadrilateral element having two degrees of freedom at each node is formulated by using the concept of static condensation. It is based on the strain approach and satisfies the equilibrium equations. However any singularity is eliminated by the use of local axes optimally oriented. From several numerical examples, it is shown that satisfactory results can be obtained while using only a few numbers of finite elements. This element can be used to solve general plane elasticity problems and excellent results can be

obtained for both deflections and stresses. The results obtained are highly superior than those obtained using the standard element Q4, and are comparable with those given by the robust element Q8. The simplicity and efficiency of this element make it an excellent alternative for analyzing complex civil engineering problems.

2. Description and formulation of the new element "Q4SBE5"

Figure 1a shows the geometry of the proposed element "**Q4SBE5**" **(Strain Based Quadrilateral Element with Four Corner Nodes and an Internal Node)** and the corresponding nodal displacements. The quadrilateral element has five nodes, four corner nodes in addition to an internal node. Each node (i) is attributed to two degrees of freedom (d.o.f) Ui, and Vi. Therefore, the displacement field should include ten independent constants.

The strain components at any point in the Cartesian coordinate system are expressed in terms of the displacements as follow:

$$\varepsilon_x = \frac{\partial U}{\partial x} \tag{1a}$$

$$\varepsilon_y = \frac{\partial V}{\partial y} \tag{1b}$$

$$\gamma_{xy} = \frac{\partial U}{\partial y} + \frac{\partial V}{\partial x} \tag{1c}$$

For the case that the strains above equal to zero, the integration of equations (1) leads to expressions of the form:

$$U = a_1 - a_3 y \tag{2a}$$

$$V = a_2 + a_3 x \tag{2b}$$

Equations (2) represent the displacement field in terms of its three rigid body displacements.

The strains in equations (1) cannot be considered independent, they are in terms of two displacements U, V and hence must satisfy the compatibility equation. This equation can be obtained by eliminating U, V from equation (1), resulting in:

$$\frac{\partial^2 \varepsilon_x}{\partial y^2} + \frac{\partial^2 \varepsilon_y}{\partial x^2} - \frac{\partial^2 \gamma_{xy}}{\partial x \partial y} = 0 \qquad (3)$$

Equations (2) require three independent constants (a_1, a_2, a_3) to account for the three components of the rigid body displacements. Therefore seven additional constants (a_4, a_5,….a_{10}) are needed to define the displacements due to straining actions. These seven independent constants can be defined as follow:

$$\begin{cases} \varepsilon_x = a_4 + a_5 y + a_9 x \\ \varepsilon_y = a_6 + a_7 x + a_{10} y \\ \gamma_{xy} = -a_5 xR - a_7 yR + a_8 - a_9 Hy - a_{10} Hx \end{cases} \qquad \text{Or } \{\varepsilon\} = [Q]\{a\} \qquad (4)$$

where: $H = \frac{2}{(1-v)}$; $R = \frac{2v}{(1-v)}$

The strains given by equation (4) satisfy the compatibility equation (3) as well as the two-dimensional equilibrium equations (5a, 5b):

$$\frac{\partial \sigma_x}{\partial x} + \frac{\partial \tau_{xy}}{\partial y} = 0 \qquad (5a)$$

$$\frac{\partial \sigma_x}{\partial y} + \frac{\partial \tau_{xy}}{\partial x} = 0 \qquad (5b)$$

By integrating equations (4) and substituting equations (2), we obtain the final displacement functions:

$$U = a_4 x + a_5 xy - a_7 y^2 (R+1)/2 + a_8 y/2 + a_9 (x^2 - H y^2)/2 \qquad (6a)$$

$$V = -a_5 x^2 (R+1)/2 + a_6 y + a_7 xy + a_8 x/2 + a_{10} (y^2 - Hx^2)/2 \qquad (6b)$$

The stiffness matrix is then calculated following well-known matrix expressions:

$$[K_e] = [A^{-1}]^T [K_0] [A^{-1}] \qquad (7a)$$

$$[K_0] = \iint_S [Q]^T [D][Q] dx.dy \qquad (7b)$$

where [A], [Q] and $[K_0]$ are derived in appendices A, B and C

and $[D] = \begin{bmatrix} D11 & D12 & 0 \\ D12 & D22 & 0 \\ 0 & 0 & D33 \end{bmatrix}$ is the usual constitutive matrix

$$D11 = D22 = \frac{E}{(1-\nu^2)}; \; D12 = \frac{\nu.E}{(1-\nu^2)}; \; D33 = \frac{E}{2(1+\nu)}$$

In this classical formulation, two problems can arise: a) the geometrical problem of distortion of finite elements of higher degrees; and b) the problem of locking for finite elements of relatively low degrees.

To avoid these problems, the strain-based approach with proper analytical integration is adopted [5].

3. Evaluation of the element stiffness matrix $[K_e]$

The element stiffness matrix $[K_e]$ is obtained using the following expression:

$$[K_e] = [A^{-1}]^T \left[\iint_S [Q]^T [D][Q] dx.dy \right] [A^{-1}] \tag{8a}$$

$[K_e]$ is a 10x10 matrix; however the 2 additional middle dofs are to be condensed out.

$$[K_e] = [A^{-1}]^T [K_0] [A^{-1}] \tag{8b}$$

With:

$$[K_0] = \iint_S [Q]^T [D][Q] dx.dy \tag{8c}$$

Since [A] and its inverse can be evaluated numerically, the key to solving the problem relies on the accurate evaluation of the integral in (8c). However, it is known that large distortions typically lead to erroneous results particularly when calculating the Jacobian. In this study, a simple expression to evaluate $[K_0]$ regardless of the degree of the polynomial of the kinematics field and the element distortion, is proposed (Fig.1b):

$$I = [K_0] = \iint_S C.x^{\alpha} y^{\beta} \, d\,x.d\,y \tag{9}$$

where x_1, x_2, x_3 and x_4 defined in Fig. 1b are the coordinates of nodes 1, 2, 3 and 4 in the X direction; and y_1, y_2, y_3 and y_4 are the functions of the quadrilateral sides, 1-2, 2-3, 3-4, 4-1 respectively.

The general solution of equation (9) for a quadrilateral is [5]:

$$I = \sum_{P=1}^{3} I_P \tag{10}$$

$$\text{With: } I_P = \frac{C}{\beta+1}\sum_{k=1}^{\beta+2}\frac{1}{k+\alpha}.C(k)\left(a_j{}^{k-1}.b_j{}^{\beta+2-k} - a_i{}^{k-1}.b_i{}^{\beta+2-k}\right)\left(x_n{}^{k+\alpha} - x_m{}^{k+\alpha}\right) \quad (11)$$

The stiffness matrix is derived directly using exact and not reduced integration.

4. Validation tests

In this section, several well-established quadrilateral plane elements are compared with the present element **"Q4SBE5"** through numerical test problems. The performance of elements for distorted shapes is also tested.

The present element is compared to the following elements:

SBRIE: the strain based rectangular in-plane element [4]

SBRIE2: The strain based rectangular in-plane element with an internal node [4]

Q4: the standard four-node isoparametric element.

Q8: the standard eight -node isoparametric element.

PS5β*: Pian and Sumihara's four*- node five-beta mixed element [6]

AQ: Cook's quadrilateral counterpart [7] *of Allman's triangle* [8]

MAQ: a mixed counterpart of AQ using complete linear stress modes for all stress components, i.e. nine stress modes are involved. Since the assumed stress space is invariant, *this element is trusted to be identical to Yunus et al's mixed* AQ [9]

Q4Rβ*:* the quasi- conforming counterpart of AQ proposed by Lin et al. [10]

Q4S: Mac-*Neal and Harder's refined membrane element with drilling* degree of freedom [11]

07β*:* the Sze element [12]

Q8: the Mac -Neal [13]

Allman element [8]

4.1. Bending of a cantilever beam (High order patch test)

In this test problem, the behaviour of finite elements with a significant geometrical distortion is examined. This problem was critically analysed in [12] to test the behaviour and accuracy of elements 07β and 07β*.

The problem consists of a cantilever beam having a rectangular section (l x t x h = 10 x 1 x 2), and subjected to two nodal forces (P =1000) forming a couple (Fig. 2a).

Figures 2b and 2c show the stability, and confirm the excellent performance of the "Q4SBE5" element regardless of the geometrical distortion (with only one element along h!). This result can be explained because of the nature of the analytical integration carried out. The results confirm that element Q4SBE5 passes the High Order Patch Test [14, 15].

The results of "Q4SBE5" are powerful and comparable with the exact solution. For the standard quadrilateral element Q4, poor precision is always detected (Figures 2b and 2c).

4.2 Mac-Neal's elongated cantilever beam

In this example, the elongated cantilever beam of Mac-Neal and Harder [13] is studied (Fig.3a). The beam has a rectangular section (6 x 2 x 1), and is subjected to a moment at the end (M=10) as well as a load applied at its tip (P=1).

The beam is modelled by six rectangular (Fig.3a), trapezoidal (Fig.3b) and parallelogram (Fig.3c) elements.

The results obtained using **Q4SBE5** are compared with those obtained using other well-known quadrilateral elements (Table 1).

In order to test the convergence of the **Q4SBE5** element, the normalised tip deflection is evaluated and compared with those computed using other elements in Figures (4, 5) for the case of four different mesh configurations.

Mac-Neal [11] noted that the trapezoidal shape of membrane finite elements with four nodes and without rotational degrees of freedom generates a locking problem, even if these elements pass the patch-test. This problem is known as "trapezoidal locking". The results obtained for elements Q4 and PS5β (Table 1) clearly confirm the problem of trapezoidal locking.

However, this phenomenon does not apply to finite elements based on the strain approach. For the three meshes (Figures 3a, 3b, 3c), it is clear that the **Q4SBE5** element does not suffer from trapezoidal locking.

In conclusion, it can be confirmed that the "Q4SBE5" element is very efficient for the case of problems dominated by bending, and that its performance remains stable with geometrical distortions.

4.3. Allman's cantilever beam

4.3.1. Distortion sensitivity study

In the next test problem, the vertical displacement V_A at the free end of a short cantilever is evaluated under the effect of a uniform vertical load with resultant W (Fig. 6a). This problem is considered by many researchers as a good test to validate the efficiency of plane elements for problems dominated by bending. The analytical solution for the vertical deflection at point A is calculated as follow [16]:

$$V_A = \frac{PL^3}{3EI} + \frac{(4+5\upsilon)}{2EH} PL = 0{,}3553 \qquad (12)$$

The results obtained for the two mesh cases (regular and distorted) are listed in Table 2.

The results in the case of the distorted mesh (Fig.6c) confirm the excellent performance of element Q4SBE5. In this case, Q4SBE5 provides more accurate results than those of elements PS5ß, MAQ, QR4b, 07ß and Q4 (Table 2), and is comparable with those given by the robust element Q8, in terms of total number of degrees of freedom.

4.3.2. Aspect ratio tests for cantilever

In addition to the above test, an additional example is included here to study the sensitivity of the present element to the variation in aspect ratio. The response of a cantilever beam to a parabolic distributed shear applied at the tip as shown in Fig.7 is considered. From the results presented in Table 3, it is found that the displacement model (Q4) gives poor results, and

requires extensive mesh refinement in order to approach the correct solution. The Q4SBE5 element however performs extremely well.

4.4. Tapered panel under end shear

This problem, proposed by Cook as a test for the accuracy of quadrilateral elements [7, 17], is another popular test problem.

The problem consists of a tapered panel with unit thickness, and with one edge subjected to a distributed shear load while the other edge is fully clamped (Fig. 8).

The panel is analysed by using 2 x 2 and 4 x 4 meshes (Figs 8a, 8b). The normalised vertical deflection Vc at point C, maximum principal stress σ_{maxA} at point A and minimum principal stress σ_{minB} at point B are presented in Table 4. Principal stresses at points A and B are calculated based on the averaged stress components of the elements sharing nodes A and B, respectively.

The results of the Q4SBE5 element are compared to those obtained using several other quadrilateral elements. It was shown that the displacements calculated using the Q4SBE5 are slightly better than those obtained using the other elements for both mesh cases (Table 4).

The results for deflections and principal stresses for the refined mesh (4x4) are in good agreement to an accurate solution given in [17] using a (32x32) mesh (error 1 %).

5. Civil engineering application (Boussinesq problem, [18])

Next we examine the Boussinesq problem in the theory of linear elasticity. In this problem, a force P is vertically applied at the center of the top surface of a semi-infinite plate. Under the assumption of plane stress conditions, the stress component σ_{xx} along the x axis is given by the following equation [16]:

$$\sigma_{xx} = -2P / \pi.x \qquad (13)$$

Due to the fact that infinite domains cannot be modelled using the finite element approximations studied so far, only a finite region of the semi-infinite domain shown in Fig.9 is modelled.

Assuming homogeneity and isotropy of the material, fixed boundary conditions has been assumed along the bottom and the right side edges. The results are shown in Fig.10 for the case where Young's modulus E =32000KN/mm^2, Poisson's ratio ν =0.25, Thickness =10 mm and applied force P = 100 N.

It can be concluded that the numerical results agree rather well with those of the analytical solution.

Conclusion

The new strain based element "Q4SBE5" is proposed for the analysis of general plane elasticity problems. It is a simple element with five nodes, four corner nodes and an internal node, and has only two degrees of freedom per node. Several numerical examples were studied to evaluate the performance of the strain-based approach. In general excellent results were obtained when compared to existing elements in the literature. In addition, it can be said that "Q4SBE5" remains stable with geometrical distortions; which is partly explained by the nature of analytical integration carried out. It has been shown that excellent finite element solutions can be obtained with the use of only a small number of elements making the element very suitable for several civil engineering applications.

References

[1] Sabir A.B., 1983. A new class of Finite Elements for plane elasticity problems, CAFEM 7th, International Conference of Structural Mechanics In Reactor Technology, Chicago.

[2] Sabir A.B., 1984. Strain based finite element analysis of shear walls. , Proceedings of the third International Conference on Tall Building. Y.K Cheung and P.K.K. Lee, eds., Hong Kong, pp. 447-453.

[3] Sabir A.B., 1985. A rectangular and triangular plane elasticity element with drilling degrees of freedom, Chapter 9 in Proceeding of the 2nd International Conference on Variational Methods in Engineering, Southampton University, Springer-Verlag, Berlin, pp. 17-25.

[4] Sabir A.B. and Sfendji A., 1995. Triangular and Rectangular plane elasticity finite elements. Thin-walled Structures 21. pp. 225-232.

[5] Hamadi D., and Belarbi M.T., 2006. Integration solution routine to evaluate the element stiffness matrix for distorted shapes". Asian Journal of Civil Engineering (Building and Housing), Vol. 7, N° 5 pp. 525 -549.

[6] Pian T.H. and Sumihara K., 1984. Rational approach for assumed stress finite elements, International Journal of Numerical Methods in Engineering, Vol. 20, pp. 1685-1695.

[7] Cook R.D., 1986. On the Allman triangle and a related quadrilateral element, Computers and Structure, Vol. 22, pp. 1065 -1067.

[8] Allman, D.J., 1988. Evaluation of the constant strain triangle with drilling rotations. International Journal of Numerical Methods in Engineering. Vol. 26, pp. 2645-2655.

[9] Yunus SM.,Saigal S. and Cook R. D., 1989. On improved hybrid finite element with rotational degrees of freedom, International Journal of Numerical Methods in Engineering, Vol. 28, pp. 785-800.

[10] Lin H., Tang L.M. and Lu H.-X, 1990. The quasi-conforming plane element with rotational degree of freedom. Computers and Structures Mechanics Applications. Chinese. Vol. 7, pp. 23-31.

[11] Mac-Neal R. H. et Harder R. L., 1988. A refined four - nodded membrane element with rotational degrees of freedom, C.S., Vol. 28, pp. 75-84.

[12] Sze K.Y., Chen W. and Cheung Y.K., 1992. An efficient quadrilateral plane element with drilling degrees of freedom using orthogonal stress modes, Computer and Structures, Vol. 42, N° 5, pp. 695-705.

[13] Mac-Neal R. H. and Harder R. L., 1985. A proposed standard set of problems to test finite element accuracy, Finite Element Anal. Des. 1, pp. 3-20.

[14] Taylor R.L., Simo J.C., Zienkiewicz O.C. and Chan A.C., 1986. The patch test: A Condition for Assessing Finite Element Convergence, International Journal of Numerical Methods in Engineering, Vol. 22, pp. 39-62.

[15] Batoz J.L. et Dhatt G., 1990. Modélisation des structures par éléments finis, Vol. 1 : élastiques, Editions Hermès, Paris.

[16] Timoshenko S. P., and Goodier J. N., 1970. Theory of Elasticity, 3rd Edition. Mc Graw-Hill, New York.

[17] Bergan P.G. & Felippa C.A., A triangular membrane element with rotational degrees of freedom, CMAME, Vol. 50, pp. 25-69, 1985.

[18] Noboru Kikuchi, Finite element methods in mechanics analysis Cambridge University Press, 1986.

Appendices

Appendix A: Matrix [Q]

$$[Q]=\begin{bmatrix} 0 & 0 & 0 & 1 & y & 0 & 0 & 0 & x & 0 \\ 0 & 0 & 0 & 0 & 0 & 1 & x & 0 & 0 & y \\ 0 & 0 & 0 & 0 & -xR & 0 & -yR & 1 & -Hy & -Hx \end{bmatrix}$$

Appendix B: Matrix [A]

$$[A]=\begin{bmatrix} 1 & 0 & 0 & 0 & 0 & 0 & 0 & 0 & 0 & 0 \\ 0 & 1 & 0 & 0 & 0 & 0 & 0 & 0 & 0 & 0 \\ 1 & 0 & 0 & a & 0 & 0 & 0 & 0 & \frac{a^2}{2} & 0 \\ 0 & 1 & a & 0 & \frac{-a^2(R+1)}{2} & 0 & 0 & \frac{a}{2} & 0 & \frac{-Ha^2}{2} \\ 1 & 0 & -b & a & ab & 0 & \frac{-b^2(R+1)}{2} & \frac{b}{2} & \frac{a^2-Hb^2}{2} & 0 \\ 0 & 1 & a & 0 & \frac{-a^2(R+1)}{2} & b & ab & \frac{a}{2} & 0 & \frac{b^2-Ha^2}{2} \\ 1 & 0 & -b & 0 & 0 & 0 & \frac{-b^2(R+1)}{2} & \frac{b}{2} & \frac{-Hb^2}{2} & 0 \\ 0 & 1 & 0 & 0 & 0 & b & 0 & 0 & 0 & \frac{b^2}{2} \\ 1 & 0 & -\frac{b}{2} & \frac{a}{2} & \frac{ab}{4} & 0 & -\frac{b^2}{8}(R+1) & \frac{b}{4} & \frac{a^2-Hb^2}{8} & 0 \\ 0 & 1 & \frac{a}{2} & 0 & -\frac{a^2}{8}(R+1) & \frac{b}{2} & \frac{ab}{4} & \frac{a}{4} & 0 & \frac{b^2-Ha^2}{8} \end{bmatrix}$$

Appendix C: Matrix $[K_0]$

$$[K_0]=\begin{bmatrix} 0 & 0 & 0 & 0 & 0 & 0 & 0 & 0 & 0 & 0 \\ & 0 & 0 & 0 & 0 & 0 & 0 & 0 & 0 & 0 \\ & & 0 & 0 & 0 & 0 & 0 & 0 & 0 & 0 \\ & & & H_1 & H_2 & H_3 & H_4 & 0 & H_5 & H_6 \\ & & & & H_7 & H_8 & H_9 & H_{10} & H_{11} & H_{12} \\ & & & & & H_{13} & H_{14} & 0 & H_{15} & H_{16} \\ & & & & & & H_{17} & H_{18} & H_{19} & H_{20} \\ & & & & & & & H_{21} & H_{22} & H_{23} \\ & & & & & & & & H_{24} & H_{25} \\ & & & & & & & & & H_{26} \end{bmatrix}$$

$$H_1 = abD_{11} \qquad H_{10} = -\frac{1}{2}Rba^2D_{33} \qquad H_{19} = \frac{1}{3}\left(ba^3D_{12} + ab^3RHD_{33}\right)$$

$$H_2 = \frac{1}{2}ab^2D_{11} \qquad H_{11} = \frac{a^2b^2}{4}\left(RHD_{33} + D_{11}\right) \qquad H_{20} = \frac{a^2b^2}{4}\left(RHD_{33} + D_{22}\right)$$

$$H_3 = abD_{12} \qquad H_{12} = \frac{1}{3}\left(ab^3D_{12} + ba^3RHD_{33}\right) \qquad H_{21} = abD_{33}$$

$$H_4 = \frac{1}{2}ba^2D_{12} \qquad H_{13} = abD_{22} \qquad H_{22} = -\frac{1}{2}ab^2HD_{33}$$

$$H_5 = \frac{1}{2}ba^2D_{11} \qquad H_{14} = \frac{1}{2}ba^2D_{22} \qquad H_{23} = -\frac{1}{2}ba^2HD_{33}$$

$$H_6 = \frac{1}{2}ab^2D_{12} \qquad H_{15} = \frac{1}{2}ba^2D_{12} \qquad H_{24} = \frac{1}{3}\left(ab^3H^2D_{33} + ba^3D_{11}\right)$$

$$H_7 = \frac{1}{3}\left(ab^3D_{11} + ba^3R^2D_{33}\right) \qquad H_{16} = \frac{1}{2}ab^2D_{22} \qquad H_{25} = \frac{a^2b^2}{4}\left(H^2D_{33} + D_{12}\right)$$

$$H_8 = \frac{1}{2}ab^2D_{12} \qquad H_{17} = \frac{1}{3}\left(ba^3D_{22} + ab^3R^2D_{33}\right) \qquad H_{26} = \frac{1}{3}\left(ba^3H^2D_{33} + ab^3D_{22}\right)$$

$$H_9 = \frac{a^2b^2}{4}\left(R^2D_{33} + D_{12}\right) \qquad H_{18} = -\frac{1}{2}ab^2RD_{33}$$

Where: $D11 = D22 = \frac{E}{\left(1-\nu^2\right)}$; $D12 = \frac{\nu.E}{\left(1-\nu^2\right)}$; $D33 = \frac{E}{2\left(1+\nu\right)}$;

With: $H = \frac{2}{\left(1-v\right)}$; $R = \frac{2v}{\left(1-v\right)}$

a and b are the element dimensions for the rectangular shape

Table 1 Normalised tip deflection for Mac-Neal's elongated beam

Element	Pure bending			End shear		
	Regular	Trapezoidal	Parallel	Regular	Trapezoidal	Parallel
Q4	0,093	0,022	0,031	0,093	0,027	0,034
PS5β (Pian, 4)	1,000	0,046	0,726	0,993	0,052	0,632
AQ (Cook, 86)	0,910	0,817	0,881	0,904	0,806	0,873
MAQ (Yun, 89)	0,910	0,886	0,890	0,904	0,872	0,884
Q4 (Mac,89)	-	-	-	0,993	0,986	0,988
07β (Sze, 92)	1,000	0,998	0,992	0,993	0,988	0,985
Q4SBE5	**1,000**	**1,000**	**1,000**	**0,993**	**0,994**	**0,994**
Theory	**1,000 (0,270)**			**1,000 (0,1081)**		

Table 2 Allman's short cantilever beam, Normalised vertical displacement at point A

Formulation/ Element	Mesh	Normalized vertical displacement at A
Allman (All., 88)	Reg.	0,852
Allman (All., 88)	Dist.	-
PS5β (Pian, 84)	Reg.	0,978
PS5β (Pian, 84)	Dist.	0,925
AQ(Cook, 86)	Reg.	0,918
AQ(Cook, 86)	Dist.	0,947
MAQ(Yunus et al., 89)	Reg.	0,918
MAQ(Yunus et al., 89)	Dist.	0,952
QR4β (Lin. et al., 90)	Reg.	0,978
QR4β (Lin. et al., 90)	Dist.	0,977
07β (Sze et al., 92)	Reg.	0,978
07β(Sze et al., 92)	Dist.	0,978
Q4	Reg.	0,679
Q4	Dist.	0,596
Q8 (Mac., 88)	Reg.	**0,985**
Q8 (Mac., 88)	Dist.	**0,994**
Q4SBE5	Reg.	**0,983**
Q4SBE5	Dist.	**0,995**
Exact solution (Timoshenko, 1970)		**1,000 (0,3553)**

Table 3 Normalized deflection at point A, of a cantilever beam under a tip load

Element aspect ratio a/b	Normalised tip deflection			
	1.0	0	4.0	8.0
Mesh	2 x 8	2 x 4	2 x 2	2 x 1
SBRIE	0.972	0.957	0.905	0.738
Q4	0.888	0.699	0.378	0.134
SBRIE2	0.97	0.922	0.836	0.666
Q4SBE5	**0.988**	**0.973**	**0.922**	**0.750**
Analyt.	**1.000 (0.3558)**			

Table 4 Normalised prediction for tapered panel under end shear

Element model	2 x 2 mesh			4 x 4 mesh		
	V_C	σ_{maxA}	σ_{minB}	V_C	σ_{maxA}	σ_{minB}
Q4	0,496	0,437	0,533	0,766	0,756	0,719
AQ (Coo., 86)	0,890	0,780	0,900	0,965	0,936	1,010
Ref. (All., 88)	0,848	0,771	0,856	0,953	0,956	0,997
FRQ (Aya., 93)	0,914	0,741	0,775	0,973	0,932	0,985
PS5β (Pian, 84)	0,884	0,786	0,771	0,963	0,950	0,924
MAQ (Yun, 89)	0,890	0,779	0,886	0,965	0,941	0,967
QR4β (Lin, 90)	0,941	0,879	1,059	0,980	0,990	0,997
Ref. (Ber., 85)	0,852	0,720	0,898	0,938	0,902	0,849
Ref.(Ibr., 90)	0,865	-	-	0,962	-	-
Ref. (Sim., 89)	0,884	-	-	0,963	-	-
07β (Sze, 92)	0,945	0,835	1,069	0,981	0,982	1,012
Q4SBE5	**1,0652**	**1,508**	**1,171**	**1,011**	**1,004**	**0,992**
32 x 32 mesh Ref. [Ber., 85]	1,000 (23,90)	1,000 (0,236)	1,000 (-0,201)	1,000 (23,90)	1,000 (0,236)	1,000 (-0,201)

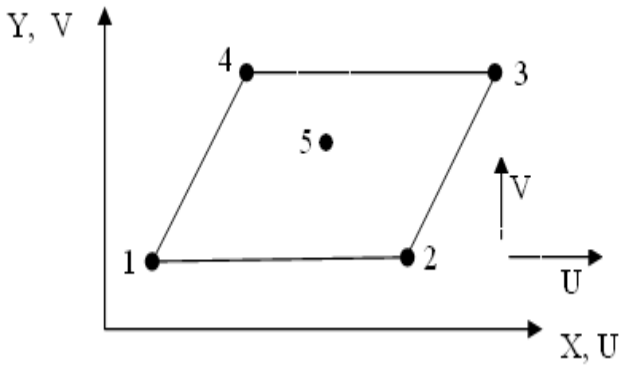

Fig.1a: Co-*ordinates and nodal points for the element"* **Q4SBE5**

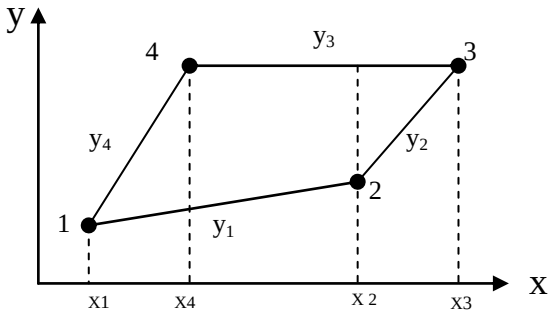

Fig.1b: Quadrilateral element

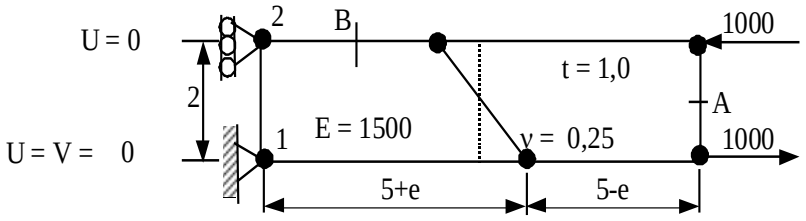

a) Pure Bending of a Cantilever beam; Data and Meshes

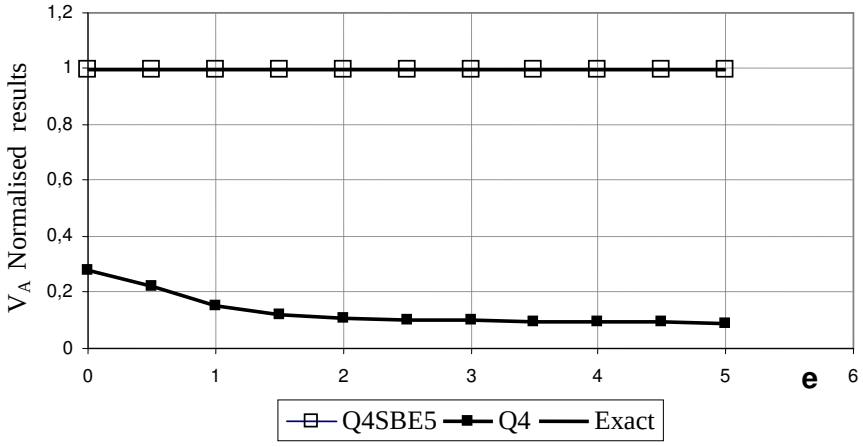

b) Vertical Displacement at Point A. Normalised results

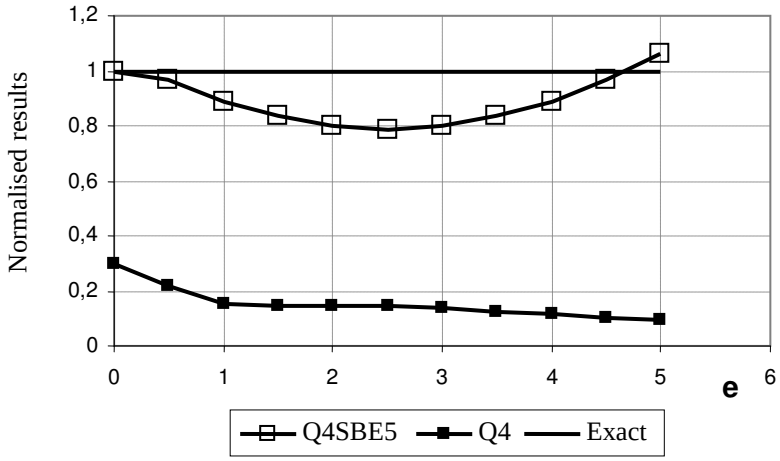

c) Normal stress at Point B. Normalised results

Fig.2. Pure bending of a cantilever beam

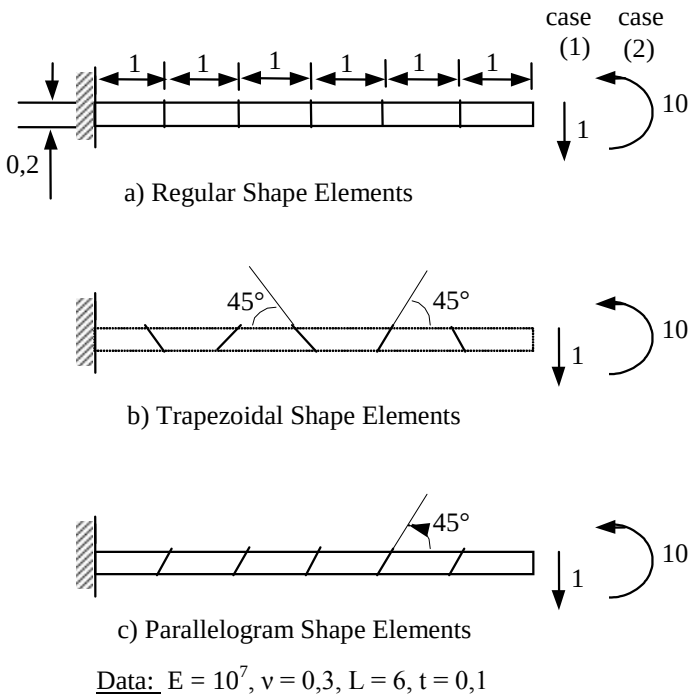

Fig.3 Mac-Neal's elongated beam subject to (1) end shear and (2) end bending.

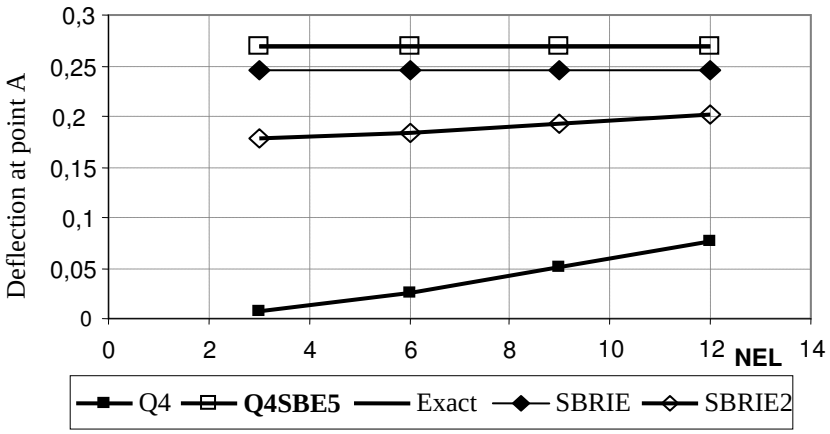

NEL= Number of elements

Fig.4 Convergence Curves for deflection at point A
Mac- *Neal's cantilever beam* under pure bending

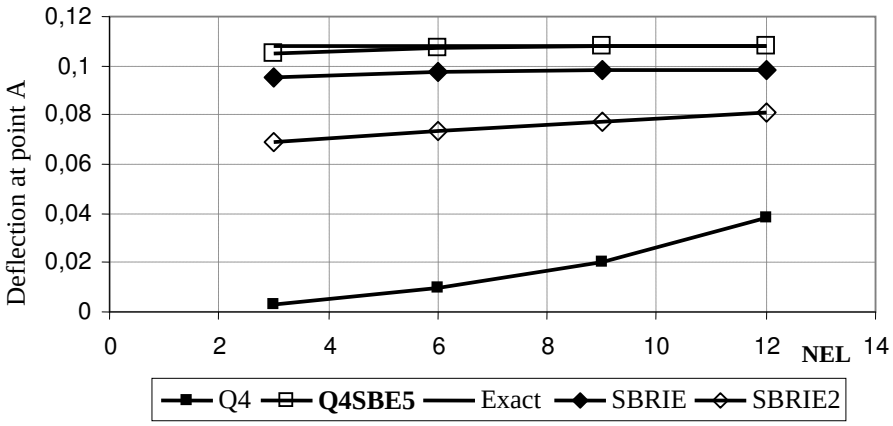

Fig.5 Convergence Curves for deflection at point A
Mac-*Neal's* cantilever beam under end shear

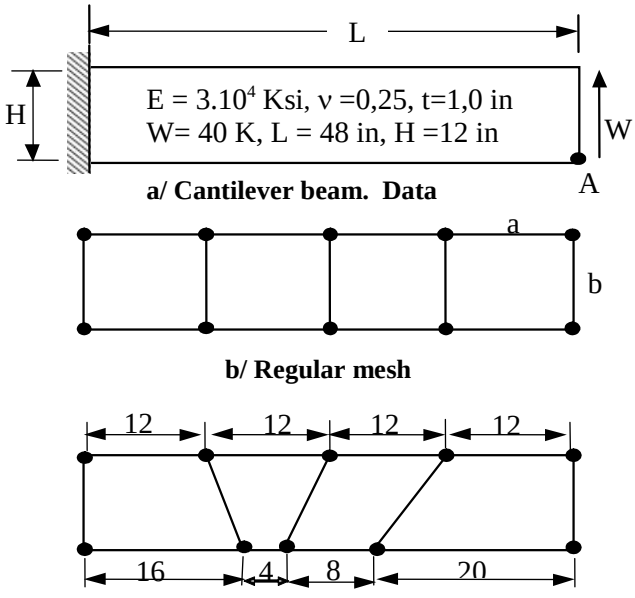

Fig.6 Allman's cantilever beam; Data and mesh

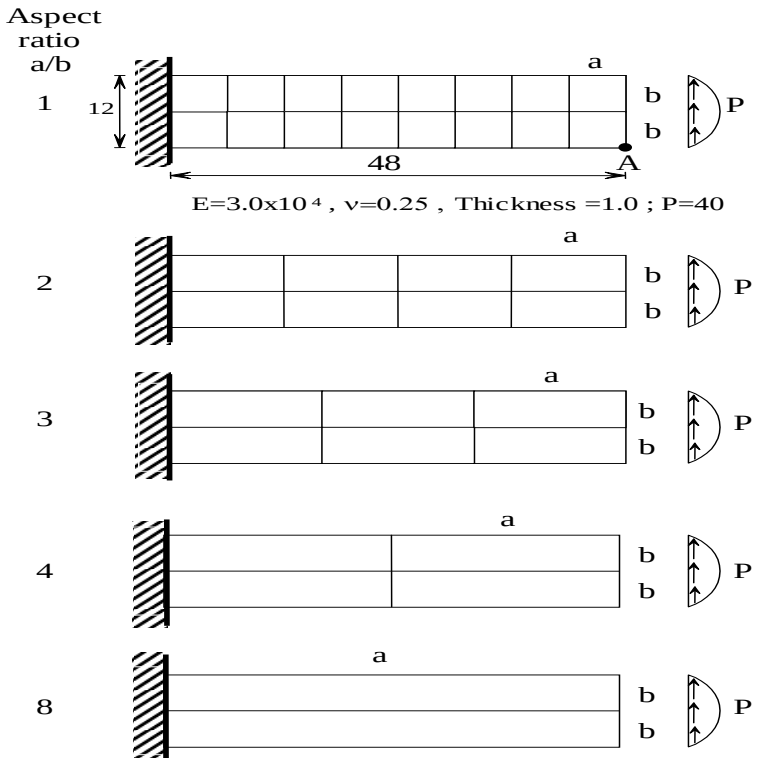

Fig.7 Cantilever beam subjected to parabolically distributed shear
Aspect ratio tests

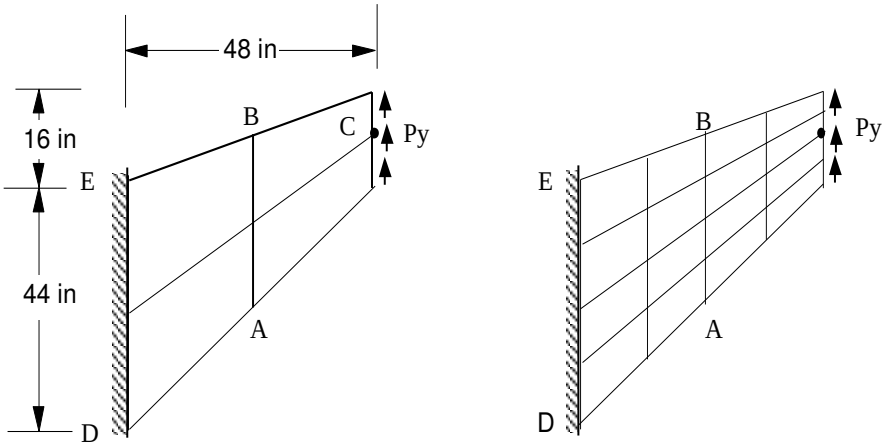

(a) 2 x 2 mesh (b) 4 x 4 mesh

Thickness t =1 in; Py = 1 pi (uniformly distributed load)

Boundary conditions:
U = V = 0 (DE)

Fig.8 Tapered panel subjected to end shear; data and meshes

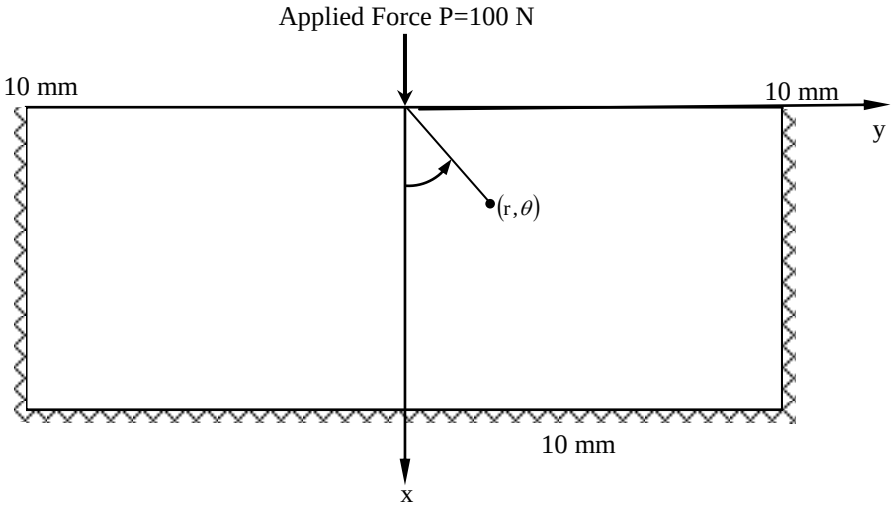

Fig.9 Domain for Boussinesq problem

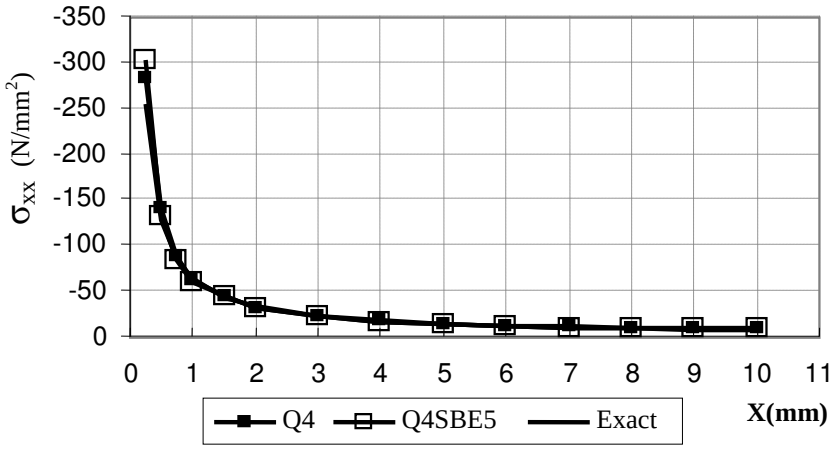

Fig.10. *Stress* σ_{xx} along x Axis $(\theta=90^0)$